Computers and Geosciences 124 (2019) 115–127

Contents lists available at ScienceDirect

Computers and Geosciences

journal homepage: www.elsevier.com/locate/cageo

Waveform-based microseismic location using stochastic optimization algorithms: A parameter tuning workflow☆

Lei Li[a,b,c], Jingqiang Tan[a,b,c,*], Yujiang Xie[d], Yuyang Tan[e], Jan Walda[d], Zhengguang Zhao[f], Dirk Gajewski[d]

[a] Key Laboratory of Metallogenic Prediction of Nonferrous Metals and Geological Environment Monitoring (Central South University), Ministry of Education, 410083, Changsha, China
[b] Hunan Key Laboratory of Nonferrous Resources and Geological Hazard Exploration, 410083 Changsha, China
[c] School of Geosciences and Info-Physics, Central South University, 410083, Changsha, China
[d] Institute of Geophysics, University of Hamburg, D-20146, Hamburg, Germany
[e] School of Earth and Space Sciences, University of Science and Technology of China, 230026, Hefei, China
[f] School of Earth and Environmental Sciences, The University of Queensland, QLD, 4072, Brisbane, Australia

ARTICLE INFO

Keywords:
Data processing
Algorithms
Geophysics
Inverse problems

ABSTRACT

A fast and accurate source location estimation is the foundation for passive seismic processing and interpretation. Waveform-based location methods become more and more popular for analysis of both natural and induced seismicity. We utilize stochastic optimization algorithms to speed up microseismic location. Two waveform-based location methods (i.e. diffraction stacking and cross correlation stacking) are adopted to test the performance of three algorithms (i.e. particle swarm optimization, differential evolution, and neighbourhood algorithm). In order to enhance the algorithmic performance, we propose a parameter tuning workflow which consists of two types of repeated tests. One type is multiple independent tests for a single event and the other involves tests of multiple events. The success rate, speedup, location uncertainty and bias are investigated to assess the algorithmic performances. We apply the workflow to a field dataset of mining induced seismicity and obtain preferential algorithm(s) with optimized ranges of control parameters. Synthetic tests are also conducted to demonstrated the feasibility of the proposed parameter tuning workflow. Given the two imaging operators, differential evolution is demonstrated to be the preferential one accounting for both algorithmic robustness and efficiency. Meanwhile, the workflow also examines the characteristics of different imaging operators. Cross correlation stacking proves to be simpler and more robust than its counterpart. Though the workflow is developed for microseismic location, it can also be adapted for other seismic inversion problems (e.g., source mechanism inversion) and ensure the algorithmic robustness and efficiency.

1. Introduction

Seismic location problem is a classic inverse problem in geophysics and seismology. A fast and accurate source location estimation is fundamental for analysis of both natural and induced seismicity. Take shale gas production as an example, both field and laboratory studies have shown hydraulic fracturing could induce a large amount of microseismic/acoustic emission events (Maxwell, 2014; Shapiro, 2015; Lyu et al., 2018a, 2018b). Microseismic monitoring is now a basic tool for reservoir monitoring and characterization (Maxwell, 2014; Grechka and Heigel, 2017; Li et al., 2019). The temporal and spatial distribution of microseismic events is used to delineate the geometry and evolution of subsurface fractures, thus source location is the most fundamental procedure of microseismic monitoring. Due to the low signal-to-noise ratio (SNR) and large amounts of microseismic data, waveform- or migration-based location methods have been proposed and applied in different scales of seismology, such as tectonic tremor and earthquake (Kao and Shan, 2004; Drew et al., 2013; Grigoli et al., 2016; Poiata et al., 2016), mining induced seismicity (Grigoli et al., 2014; Hassanil et al., 2018), and microseismic monitoring in reservoirs (Duncan and

☆ Code availability section: The reference source codes are available in MATLAB on GitHub at https://github.com/leileely/microseismic_stochastic.

* Corresponding author. Key Laboratory of Metallogenic Prediction of Nonferrous Metals and Geological Environment Monitoring (Central South University), Ministry of Education, 410083, Changsha, China.

E-mail addresses: leileely@126.com (L. Li), tanjingqiang@gmail.com (J. Tan), yujiangxie@gmail.com (Y. Xie), tanyy0@ustc.edu.cn (Y. Tan), jan.walda@uni-hamburg.de (J. Walda), zhengguang.zhao@uq.net.au (Z. Zhao), dirk.gajewski@uni-hamburg.de (D. Gajewski).

https://doi.org/10.1016/j.cageo.2019.01.002
Received 1 August 2018; Received in revised form 15 November 2018; Accepted 7 January 2019
Available online 11 January 2019
0098-3004/

Nomenclature

GA	Genetic algorithm
PSO	Particle swarm optimization
SA	Simulated annealing
VFSA	Very fast simulated annealing
ANN	Artificial neural network
NA	Neighbourhood algorithm
DE	Differential evolution
FGS	Full grid search
CMA-ES	Covariance matrix adaptation evolution strategy
SNR	Signal-to-noise ratio
CRS	Common-reflection surface
DS	Diffraction stacking
CCS	Cross correlation stacking
STA/LTA	Short-term-average to long-term-average
NASD	Normalized average standard deviation
NAF	Normalized average fitness
M_W	Moment magnitude
M_L	Local magnitude
S_{DS}	Diffraction stacking value
S_{CCS}	Cross correlation stacking value
u	Origin time
C	Input waveform
$t_{\max}$, $T_{\max}$	Length of time samples
N	Number of receivers
δ	Dirac delta function
$\mathbf{x}$	Source position vector (x, y, z)
V_p	P-wave velocity
w	Inertia weight
c_1, c_2	Acceleration constants
CR	Crossover parameter
F	Differential weight
n_r	Number of resampled Voronoi cells
NP	Size of population/candidates
NG	Number of generations/iterations
SR	Success rate
T_F	Computation time of full grid search
T_O	Computation time of the optimization algorithm

Eisner, 2010; Zeng et al., 2014). Waveform-based methods are modified from migration techniques in exploration seismology, they locate the source by focusing or back-projecting the waveforms into discrete grid points with a certain imaging or migration operator, which comprises related traveltime information. Moreover, waveform-based methods do not require phase picking and can detect more weak events due to the advantage of waveform stacking (e.g. Gajewski and Tessmer, 2005; Gajewski et al., 2007; Grigoli et al., 2018).

However, a potential disadvantage of waveform stacking is the relatively large computational effort, especially for surface monitoring with large arrays and large target zones (Pesicek et al., 2014; Xue et al., 2015; Li et al., 2017). Actually, seismic location is a classical optimization problem. For waveform-based methods, the imaging function is complex and its smoothness depends on many factors, such as the imaging operator, velocity model, SNR, and receiver geometry, etc. In general, the imaging function has local extrema and a decent initial model cannot be provided, thus conventional gradient-based optimization algorithms are not very suitable. Fortunately, stochastic optimization algorithms are found to be feasible for the non-linear location problem (e.g. Ružek and Kvasnička, 2001), and improve the convergence rate to the global maximum and accuracy.

Stochastic algorithms can be classified as global optimization algorithms due to the ability to search the extremum over all the search space, though they are not guaranteed to converge to the global optimum consistently. Some of stochastic algorithms are inspired by natural laws and empirical principles. These algorithms can be categorized into evolutionary algorithms (e.g. genetic algorithm (GA)), swarm intelligence (e.g. particle swarm optimization (PSO)), simulated annealing (SA), and artificial neural network (ANN), etc. (e.g. Yang, 2010). Several stochastic algorithms have been proven to be effective for solving complicated geophysical problems. For example, Kennett et al. (2000) utilized the neighbourhood algorithm (NA) for both hypocenter and source mechanism inversion, and obtained rapid and effective results of a field event. Shaw and Srivastava (2007) reported the effectiveness of PSO in multiparameter inversion of geophysical data. Walda and Gajewski (2017), Xie and Gajewski (2017) utilized differential evolution (DE) to determine common-reflection surface (CRS) attributes. Pei et al. (2009), Zhang et al. (2014), and Tan et al. (2018a) applied SA, DE, and NA to invert microseismic velocity models, respectively. Maity et al. (2014), Maity and Salehi (2016) proposed and applied a hybrid ANN based workflow for first arrival picking of microseismic data. Luu et al. (2018) proposed a competitive PSO to escape from local extrema, and applied it in traveltime tomography associated with induced seismicity. Recently, several studies have successfully incorporated stochastic algorithms into microseismic location. Oye and Roth (2003) applied NA in 3D seismic location using P- and S-wave travel times for hydrocarbon reservoirs. Song et al. (2013) studied the DE algorithm along with Bayesian theory to improve the location accuracy and stability. Sheng et al. (2014) presented a combined algorithm of PSO and DE to overcome the side effects of inaccurate first arrival time. Lagos et al. (2014), Lagos and Velis (2018) implemented very fast simulated annealing (VFSA) and PSO in picking-based microseismic location, while Brunini et al. (2017) demonstrated the superiority of DE regarding location uncertainty and accuracy compared with VFSA and PSO. Wuestefeld et al. (2018) evaluated the performance of full grid search (FGS), OcTree, SA, and DE in locating synthetic microseismic events and found, that DE generally worked better and only FGS could provide the correct location in most cases. Besides, stochastic algorithms are also incorporated into waveform-based location method. Gharti et al. (2010) successfully incorporated DE into an envelope stacking-based method. Zimmer and Jin (2011) compared three stochastic algorithms (i.e. ABC, SA, and DE) in locating hydraulic fracturing-induced microseismicity and demonstrated that DE had the best overall performance when considering different datasets. Pesicek et al. (2014) and Verdon et al. (2017) utilized covariance matrix adaptation evolution strategy (CMA-ES) and NA in microseismic location, respectively. Li et al. (2017) analyzed the performances of PSO with two stacking operators and showed that it could largely improve the computational efficiency of waveform-based location methods.

Due to the stochastic nature of these algorithms, there is no guarantee that they will eventually converge to the global extremum. A common practice to alleviate this issue is parameter tuning for individual methods and datasets. This process helps to provide good values of parameters before running the algorithm. In fact, an extensive study of parameter tuning of stochastic algorithms for microseismic location is still missing. In this work, we aim to select an optimal stochastic algorithm along with optimized tuning parameters, which have the best comprehensive performance, in waveform-based location methods. Parameter tuning of three algorithms, namely PSO (Kennedy and Eberhart, 1995), DE (Storn and Price, 1997), and NA (Sambridge, 1999), for diffraction stacking (DS) and cross correlation stacking (CCS) are conducted. Then, the performance of different algorithms with different parameters for a certain location method are compared and analyzed. Meanwhile, the characteristics and performances of different

imaging operators are revealed through the parameter tuning process as well. Our tests show that the proposed parameter tuning workflow can provide preferential algorithm(s) with optimized control parameters. Among the three algorithms, DE is demonstrated to be the preferential one, accounting for both algorithmic robustness and efficiency.

2. Theory and method

2.1. Waveform-based location methods

Waveform-based methods locate the source by focusing or back-projecting the waveforms with a certain imaging operator, which requires traveltime information. We study diffraction stacking (DS) and cross correlation stacking (CCS) in this work. DS makes use of the one-way traveltime, while CCS stacks the cross correlation waveforms along differential traveltime curves (e.g. Gajewski et al., 2007; Li et al., 2018a). The imaging functions of DS and CCS are shown in eq. (1),

$$\begin{cases} S_{DS}(\mathbf{x}, t_0) = \sum_{i=1}^{N} \sum_{\tau=0}^{t_{\max}} u(\tau, i)\delta(\tau - \tau_{i,\mathbf{x}}); \\ C(\tau, i, j) = \sum_{t_i=0}^{t_{\max}} u(t_i, i)u(t_i + \tau, i), \\ S_{CCS}(\mathbf{x}) = \sum_{i=1}^{N} \sum_{j=i+1}^{N} \sum_{\tau=0}^{t_{\max}} C(\tau, i, j)\delta(\tau - (\tau_{i,\mathbf{x}} - \tau_{j,\mathbf{x}})); \end{cases} \quad (1)$$

where S_{DS} and S_{CCS} are DS and CCS values, t_0 is the origin time, u, C are the input waveforms and the corresponding cross correlation waveforms, $t_{\max}$, $T_{\max}$ are the length of their time samples, N is the number of receivers, δ is the Dirac delta function and $\tau_{i,\mathbf{x}}$ is the traveltime for the considered velocity model from source position $\mathbf{x}$ to receiver i. It is worth noting that the imaging function of CCS is independent on the origin time t_0, while four variables (x, y, z, t_0) are involved in DS. Therefore, CCS is supposed to have better convergence ability than DS.

2.2. Stochastic optimization algorithms

Particle swarm optimization (PSO) was firstly proposed by Kennedy and Eberhart (1995). It is a global optimization algorithm based on

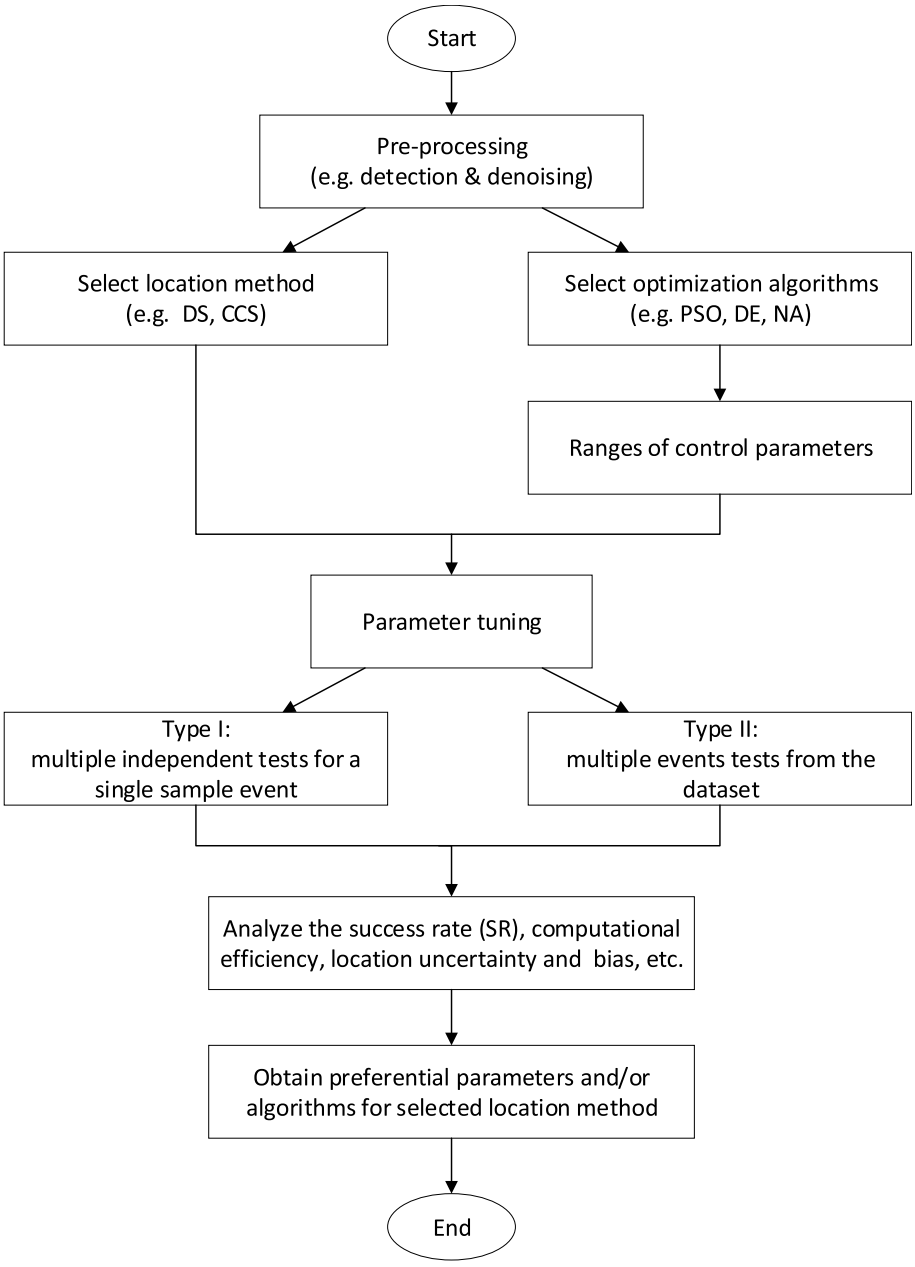

Fig. 1. Parameter tuning workflow of optimization algorithm for microseismic location.

swarm intelligence. PSO was originally inspired by the social behavior in a flock or swarm of birds and fishes searching for food. The cognitive knowledge and social behavior provide an evolutionary advantage by guiding the movement of the entire swarm from disorder to order, and finally to an optimal solution. There are four control parameters of standard PSO (Shi and Eberhart, 1998): inertia weight w, two acceleration constants c_1 and c_2, and the number of particles NP.

Differential evolution (DE) was proposed by Storn and Price (1997) and can be classified as an evolutionary algorithm. DE consists of four major operations: initialization, mutation, crossover, and selection, and three control parameters: crossover parameter CR, differential weight F, and size of population NP. Different from other evolutionary algorithms, DE adopts a simple difference-based mutation operation and a one-to-one competing strategy, which reduce the complexity of genetic operations, but retain the global search capability and have better convergence and stability.

Neighbourhood algorithm (NA) was proposed by Sambridge (1999) as a distinct stochastic algorithm for geophysical inversion. The main idea of NA is the self-adaptive sampling of parameter space with Voronoi cells, which is defined as the nearest region of one sample by a particular distance measurement. In NA, the fitness value of a sample is to the corresponding Voronoi cell, and an approximation of the misfit function is yielded. There are only two control parameters of NA: number of samples generated in each iteration NP, and number of resampled Voronoi cells n_r.

In general, stochastic optimization algorithms involve two iterative procedures: exploration (diversification) and exploitation (intensification), which are directly influenced by related control parameters (Trelea, 2003; Yang, 2010). Exploration is the ability to diversify the search globally within the problem space to find an optimum. Exploitation is the ability to intensify the search locally around a promising candidate solution to locate the optimum precisely.

Detailed descriptions and the pseudo-codes of the three stochastic optimization algorithms for microseismic location are shown in Appendix A.

2.3. Algorithm implementation

The waveform-based location problem can be stated as the following global optimization problem,

$$\begin{cases} \max\{S(\mathbf{x})\},\ \mathbf{x} = (x, y, z, t_0)^T, \\ subject\ to\ \mathbf{x}^{\min} < \mathbf{x} < \mathbf{x}^{\max}, \end{cases} \tag{2}$$

where $S(\mathbf{x})$ is the imaging function, $\mathbf{x}$ are the source parameters, including spatial coordinates (x, y, z) and origin time t_0, $\mathbf{x}^{\min}$, $\mathbf{x}^{\max}$ are the lower and upper limits of $\mathbf{x}$. When combined with microseismic location, candidates in stochastic algorithms represent the potential sources, the parameter vectors of candidates are the source parameters, the fitness/objective function is the corresponding imaging function $S(\mathbf{x})$, e.g. S_{DS} or S_{CCS} described in equation (1). More implementation details can be found in Appendix A.

The control parameters influence the performance of the algorithm (e.g. computational effort) dramatically. Although there are various empirical guidelines on how to set these parameters, stochastic algorithms are problem- and dataset-dependent. In general, two major approaches are utilized to set control parameters: parameter tuning and parameter control. The former approach involves finding good values of the parameters first and then running the algorithm using fixed values, while the latter is to adapt the control parameters during the process of optimization (Eiben et al., 1999). Though parameter control is more flexible and self-adaptive, which is also close to the nature of optimization algorithms, it will introduce new parameters and more complexity. Thus, we argue that fixed parameters obtained from parameter tuning are effective for the low-dimensional location problem. Through the tuning process, we can not only obtain an optimal algorithm along with related parameters for the respective location method, but also reveal the performances of different location methods.

In this work, we conduct the parameter tuning process as follows: (1) obtaining the ranges of parameter values based on existing references (e.g. Storn and Price, 1997; Sambridge, 1999; Das and Suganthan, 2011; Eiben and Smit, 2011) and preliminary tests; (2) parameter tuning of the three algorithms (i.e. PSO, DE, and NA) for cross correlation stacking (CCS) and diffraction stacking (DS), analyzing the performance of each algorithm with different parameters; (3) comparing the performance of DS and CCS with a common algorithm. Fig. 1 outlines the main processes of the parameter tuning workflow. In order to fairly evaluate the performances (including robustness and efficiency) of stochastic optimization algorithms, repeated tests are usually necessary to mitigate the stochastic nature. Here we conduct two types of repeated tests. The first involves performing 100 independent tests for a single sample event (as shown in Fig. 2c). The second involves locating all the 100 events selected from the dataset. We investigate the success rate (SR), computational efficiency, location uncertainty and bias in order to assess the algorithmic performances. SR is defined as the percentage of tests which find the true global extremum, and it denotes the robustness or reliability of the algorithm. Computational efficiency is denoted by speedup, which is defined by T_F/T_O, where T_F, T_O are the computation time of FGS and the optimization algorithm, respectively. A Jackknife test is used to estimate the location uncertainty of a sample event. The event is located 100 times by removing two random stations

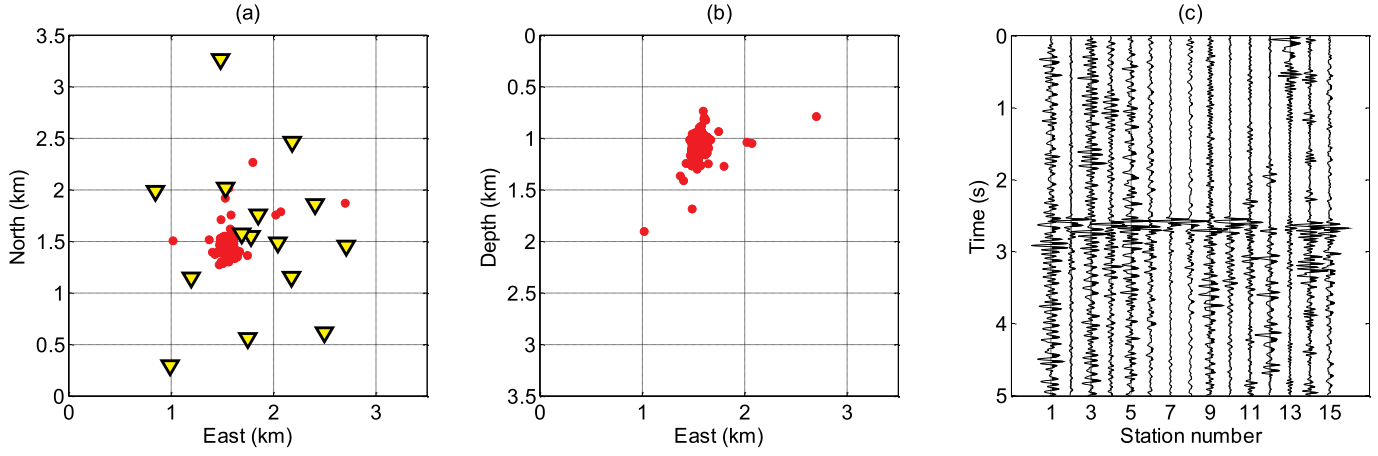

Fig. 2. (a) Monitoring geometry and top view of the 100 selected events, yellow reverse triangles are stations and red dots are events; (b) East-depth plane; (c) Band-pass filtered vertical component of a sample event. (For interpretation of the references to color in this figure legend, the reader is referred to the Web version of this article.)

at each time, and the standard deviation of Euclidean distance among the 100 locations is taken as the location uncertainty. We can always find 'the true global extremum' with full grid search (FGS). However, in field application it does not necessarily corresponds to the true source location. In this work, the location result of FGS is set as the reference to investigate the location bias.

To simplify and clarify the analysis, a fixed number of generations/iterations (NG) is selected as the convergence condition for all algorithms. Thus, NG also needs tuning and the number of cost function evaluations is also fixed when considering a certain population size. Table 1 lists the control parameters of three algorithms studied in this work. For PSO and DE, the computation time is proportional to NG since computation time for each generation remains the same. Our previous study has already shown that [0.4, 0.6] and [0.8, 1] are good reference ranges of F and CR for both DS and CCS, and higher CR can generally produce higher SR (Li et al., 2018b). Here we only study two groups of [F CR] combinations, [0.5 0.5] and [0.5 0.9]. For NA, the convergence speed is quite fast and the computation time for each generation increases as the optimization process advances (see Figs. 3–6). A large number of generations will lead to a large amount of computation time and very low speedup. Moreover, NP in NA should be proportional to n_r(Sambridge, 1999). According to above considerations, NA tests using $NG = 100$ and $NP = 30$ are omitted.

3. Field data example

In this section, we test above algorithms on a field dataset associated with mining induced seismicity monitored by the HAMNET network (Bischoff et al., 2010). The HAMNET network consists of 15 surface stations. We select 100 weak events (M_L magnitude $= -0.8$) from the dataset for our study. Only P-waves in vertical components are considered in the location process. Fig. 2a and b shows the distribution of surface stations and the 100 selected events, which are located by traveltime inversion with a manual phase picking. Fig. 2c shows the band-pass filtered vertical component of a sample event. Here we use the short-term average to long-term average (STA/LTA) (Allen, 1978) traces as the input waveforms to eliminate the side effects of polarity changes. The calculation of STA/LTA traces is consistent with that in Li et al. (2018a). The target imaging volume is 5 km × 5 km × 5 km with a grid spacing of 50 m. For diffraction stacking, we search the origin time within a time window [0, 6]s with the interval of 0.02 s, which is four times the sampling rate. A homogeneous velocity model of $V_P = 3.88$ km/s is used to calculate the traveltime table, and this model has been demonstrated to be a reasonable model for source location (e.g. Li et al., 2018a). Complete results of SR, speedup and location uncertainty are summarized in Appendix B.

3.1. Cross correlation stacking (CCS)

We first perform parameter tuning of three algorithms for CCS. Tables 2 and 3 summarize partial results of the repeated tests of a single event and 100 different events, respectively. Two types of repeated tests show nearly consistent results, which imply the repeated test of a single event can largely reflect the SR for events from the same dataset. For CCS, all the three algorithms have very high success rate (SR) and can locate the event(s) robustly. Here 'robustly' means the high consistency

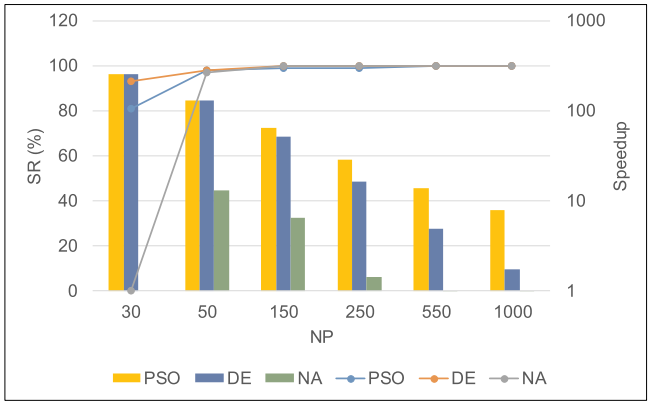

Fig. 3. SR and speedup correspond to $NG = 30$ of the single sample event. The solid lines are the SRs and the histogram are the speedup.

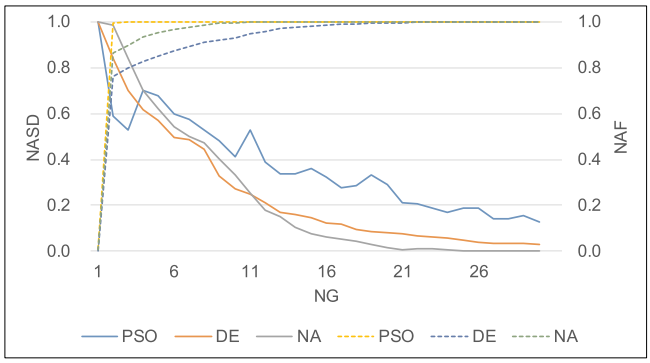

Fig. 4. Convergence speed corresponds to ($NP = 50$, $NG = 30$) of the single sample event. The solid lines are NASD and dashed lines are NAF.

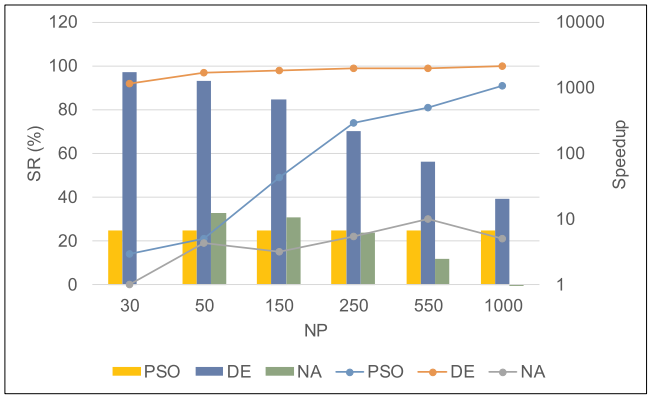

Fig. 5. SR and speedup correspond to $NG = 100$ of the 100 events. The solid lines are the SRs and the histogram are the speedup.

of location results between full grid search (FGS) and the optimization algorithm. The control parameters studied here (see Table 1 and Tables B.6-B.7 in Appendix B) make little difference on SR, though small values of number of generation NG and size of population NP in particle

Table 1
Control parameters of the studied stochastic optimization algorithms.

	PSO	DE	NA
NP	[30 50 100 250 550 1000]	[30 50 100 250 550 1000]	[50 100 250 550 1000]
NG	[30 50 100]	[30 50 100]	[30 50]
Other parameters	$c1 = c2 = 2w = \begin{bmatrix} 0.7 \\ 1{:}\,-(1-0.3)/NG{:}\,0.3 \end{bmatrix}$	$F = 0.5CR = [0.5\ 0.9]$	$n_r = [25\ 50]$

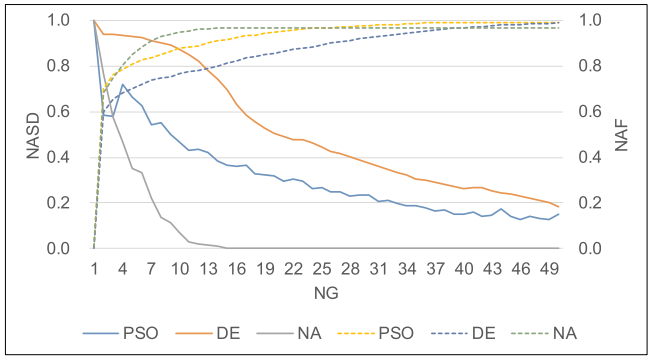

Fig. 6. Convergence speed corresponds to ($NP = 550$, $NG = 50$) of the single sample event. The solid lines are NASD and dashed lines are NAF.

Table 2
Results of SR (%) for CCS of a single event.

NP	PSO			DE			NA	
	NG (w = 0.7)			NG (F = 0.5 CR = 0.9)			NG (nr = 50)	
	30	50	100	30	50	100	30	50
30	76	100	100	91	100	100	\	\
50	98	100	100	99	100	100	93	100
100	100	100	100	100	100	100	100	100
250	100	100	100	100	100	100	100	100
550	100	100	100	100	100	100	100	100
1000	100	100	100	100	100	100	100	100

Table 3
Results of SR (%) for CCS of 100 events.

NP	PSO			DE			NA	
	NG (w = 0.7)			NG (F = 0.5 CR = 0.9)			NG (nr = 50)	
	30	50	100	30	50	100	30	50
30	81	100	100	93	100	100	\	\
50	98	100	100	98	100	100	97	100
100	99	100	100	100	100	100	100	100
250	99	100	100	100	100	100	100	100
550	100	100	100	100	100	100	100	100
1000	100	100	100	100	100	100	100	100

swarm optimization (PSO) and differential evolution (DE) result in some relatively low success rates.

Control parameters also affect the computational efficiency. We use serial codes on a computer with six cores of Intel i7-8700 3.20 GHz and 8 GB RAM to evaluate the computation time, where the FGS is the reference. It takes about 2.6 s for CCS to locate a single event with FGS. The highest speedup of particle swarm optimization (PSO), differential evolution (DE), and neighbourhood algorithm (NA) are 260, 260, and 13, respectively. Fig. 3 shows the SRs of $NG = 30$ for the 100 events (solid lines), along with corresponding speedup (histogram). The average speedup of PSO and DE for CCS is much higher than that of NA. We also investigate their convergence speed through the 100 independent tests of the single sample event. Normalized average standard deviation (NASD) and normalized average fitness (NAF) of all the candidates ($NP = 50$) over 100 independent tests versus NG are plotted in Fig. 4. All the three algorithms have close and good convergence speed. It takes less than 20 generations to converge to the global extremum. This implies that the imaging function of CCS has good convergence ability.

Table 4
Results of SR (%) for DS of a single event.

NP	PSO			DE			NA	
	NG (w = 0.7)			NG (F = 0.5 CR = 0.9)			NG (nr = 50)	
	30	50	100	30	50	100	30	50
30	1	1	16	0	10	94	\	\
50	0	7	15	0	8	100	1	9
100	0	16	46	0	8	100	15	15
250	12	43	59	1	10	100	21	16
550	25	65	73	1	27	100	20	18
1000	47	70	72	1	42	100	25	23

Table 5
Results of SR (%) for DS of 100 events.

NP	PSO			DE			NA	
	NG (w = 0.7)			NG (F = 0.5 CR = 0.9)			NG (nr = 50)	
	30	50	100	30	50	100	30	50
30	0	2	14	0	4	92	\	\
50	0	10	21	0	5	97	0	19
100	4	35	49	0	9	98	20	15
250	19	59	74	0	17	99	13	22
550	36	79	81	0	33	99	25	30
1000	65	83	91	0	35	100	29	21

3.2. Diffraction stacking (DS)

Then we perform parameter tuning of the three algorithms for DS. Tables 4 and 5 show partial results of the repeated test of a single event and 100 different events, respectively. Similar to results of cross correlation stacking (CCS), nearly consistent results from two types of repeated tests indicate the repeated test of a single event can largely reflect the SR for events from the same dataset. However, the three algorithms have much lower SR than that of CCS, which is mainly caused by the complexity of imaging function of DS. The SR of PSO increases gradually with both NP and NG reaches 91% for the 100 field events, while SR of NA is limited to about 20–30% for both types of repeated tests. The low SR of NA suggests its weak exploration ability, and there is no escaping strategy of NA when it gets trapped in local extrema. Fortunately, DE (with $F = 0.5$, $CR = 0.9$) still has SR of nearly 100% when $NG = 100$.

It takes about 88.9 s for DS to locate a single event with FGS. The highest speedup of PSO, DE, and NA are about 20, 2000, and 20, respectively. The average speedup of DE for is much higher than that of PSO and NA. Similar to Figs. 3 and 4, SR, speedup, and convergence speed of the three optimization algorithms for DS are depicted in Figs. 5 and 6. The three algorithms show distinct SRs and convergence speed. Compared with CCS, the convergence speed of DS is slower due to the additional variable, origin time t_0. Though much more candidates ($NP = 550$) are used here, it still needs about 40 generations for PSO and DE to converge to the global extremum. NA has the highest convergence speed, while it holds the lowest SR.

3.3. Comprehensive analysis

To further confirm the feasibility of these algorithms, a synthetic event generated with the station layout in Fig. 2a and a layered velocity model is relocated using the parameter ranges in Table 1. Detailed descriptions of the synthetic event and the velocity model can be found in Figs. 5 and 6 in Li et al. (2018a). Only strong S-waves in horizontal components are utilized to locate this event. The results of synthetic tests are basically consistent with those of field data examples (See Tables B.6, B.8, B.10, B.11). Actually, field and synthetic examples in

this work can be regarded as independent tests. The performance of optimization algorithms for source location problem is dependent on the complexity of the search space, but independent on that source location is true/known or not.

The convergence performance is determined by the tradeoff between the two iterative procedures of the algorithm (i.e. exploration and exploitation). This is illustrated in Figs. 5 and 6, where a large *NG* promises the high SR (orange solid line in Fig. 5) of DE through a relatively slow convergence speed (i.e. an extensive exploration process, orange solid line in Fig. 6), while the high computational efficiency of DE (blue histogram in Fig. 5) is still guaranteed. The results also indicate, that *NG* has a larger impact on the performance of DE than *NP* (Li et al., 2018b). For PSO, the SR is improved significantly as the *NP* (blue solid line in Fig. 5) and *NG* increase, while its speedup retains steady. According to Table B.12 in Appendix B, the computation time is influenced by both *NP* and *NG* of PSO for CCS, while it is only dependent on *NG* for DS. This indicates that the additional computation time from additional *NP* of PSO is important for cheap objective functions as CCS (~2.6 s), while it can be ignored for expensive objective functions like DS (~88.9 s). For NA, the resampling strategy results in high convergence speed but low SR for DS, which indicates that the strong exploitation ability in NA deviates the solution to local extremum.

Following above parameter tuning tests, we can select good control parameters for these algorithms. According to results shown in Appendix B, ($w = 0.7$) , ($F = 0.5$, $CR = 0.9$), and ($n_r = 50$) are selected for PSO, DE, and NA, respectively. ($NP = 50$, $NG = 30$), ($NP = 550$, $NG = 50$) are used for CCS and DS, respectively. These parameters are utilized to locate the sample event in Fig. 2c. The imaging results of CCS and DS are shown in Figs. 7 and 8. The optimization algorithm can improve the efficiency of waveform-based location methods by approaching the source area quickly, while skipping or abandoning most trivial imaging grids. The location uncertainty of the sample event for CCS and DS are 83.57 m and 378.59 m, respectively. The DS method has higher location uncertainty due to its extra variable (origin time t_0) compared with CCS. The uncertainties are acceptable when considering the dominant frequency (about 20 Hz) and the spacing grid (50 m). The three optimization algorithms along with selected parameters are also tested for estimating the location uncertainty. Comparing the results shown in Tables B.6, B. 8, B.13, a good correlation can be found between SR and accuracy of location uncertainty. High success rates of CCS correspond to consistent and stable location uncertainty (about 80 m), while relatively low success rates of DS relate to inaccurate and disperse location uncertainty (ranges from 250 m to 1600 m). DE has the highest location stability among the three algorithms.

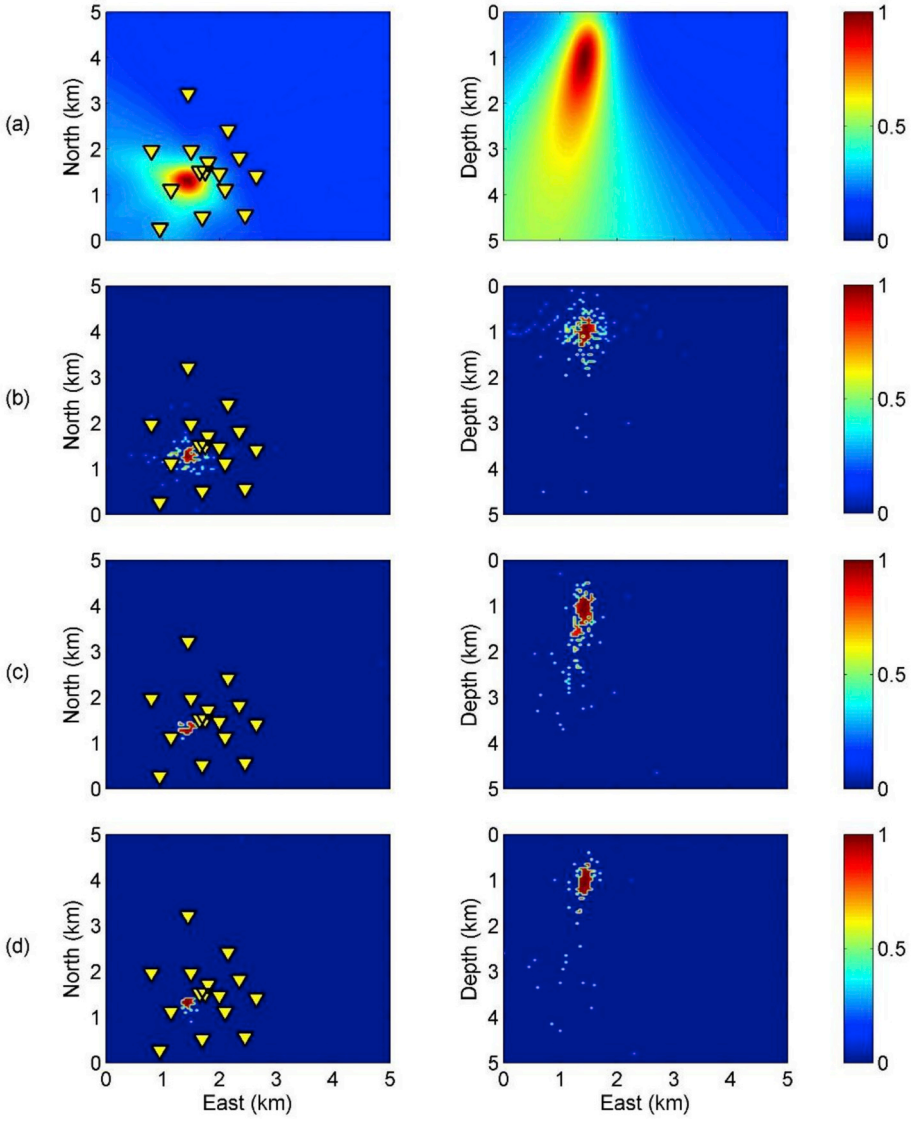

Fig. 7. Imaging results of CCS. (a) FGS; (b) PSO; (c) DE; (d) NA. The imaging results are squared and normalized according to individual maximum values.

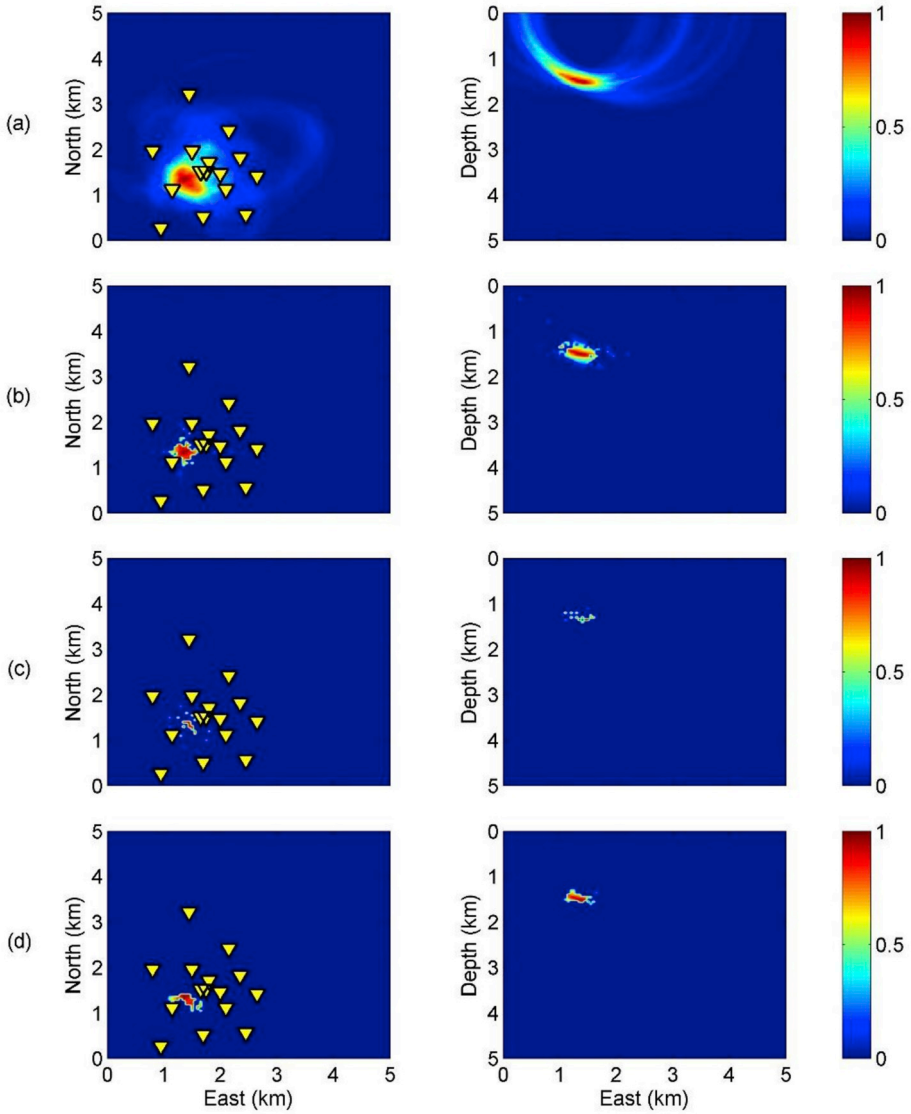

Fig. 8. Imaging results of DS. (a) FGS; (b) PSO; (c) DE; (d) NA. The imaging results are squared and normalized according to individual maximum values.

Given the relatively low SR of PSO and NA for DS, location bias of the two algorithms for the 100 events is studied. Based on analysis in Section 3.3, ($NP = 550,\ NG = 50$) is a good choice for DS, ($w = 0.7$) and ($n_r = 50$) are selected for PSO and NA, respectively. The SRs corresponding to PSO and NA are 79% and 30%. Fig. 9 shows the detailed location results. The average location bias between FGS and PSO in East-, North-, and Depth-axis is [44.0 m, 24.5 m, 173.5 m], and the overall average bias is 185.7 m. The corresponding result of NA is [121.0 m, 83.5 m, 611.5 m] and 643.9 m. Higher SR of PSO naturally yields a lower location bias (higher consistency). The largest bias is in the depth direction, which results from the depth-origin time tradeoff of DS. The distribution of seismicity swarm of PSO reserves well, while that of NA is more scattered compared with results of FGS.

4. Discussion and conclusion

In this work, we conduct parameter tuning of three stochastic optimization algorithms, particle swarm optimization (PSO), differential evolution (DE), and neighbourhood algorithm (NA), for two waveform-based microseismic location methods. Stochastic optimization algorithms can improve the efficiency of microseismic location and examine (reveal) the performance of stacking operators. Our parameter tuning tests have illustrated that the convergence performance (including robustness and efficiency) of stochastic optimization algorithms strongly depends on the fitness or objective function. For cross correlation stacking (CCS), the imaging function is relatively simple and smooth, all the three algorithms can approach the global optimum fast, locate the event(s) reliably and produce quite stable location uncertainty. In this case, the control parameters make little difference. For diffraction stacking (DS), the studied algorithms perform distinctively in many aspects. PSO is average in terms of the overall convergence performance. DE shows slow convergence speed but high computational efficiency. When control parameters are well selected, the success rate (SR) of PSO and DE can exceed 90%, under the premise that the computational efficiency is also ensured. NA has limited SR and speedup, though its convergence speed is the best. To sum up, DE has the best comprehensive performance among the three algorithms, and is the preferential algorithm for both CCS and DS. It is important to stress that stochastic algorithms are problem- or function-dependent. For instance, NA has limited SR when incorporated with DS, but shows high SR with CCS in our study.

The performance of optimization algorithms is not only fitness function-dependent, but also data-dependent. Here we only investigate the algorithmic aspect of source location with one field dataset. Many

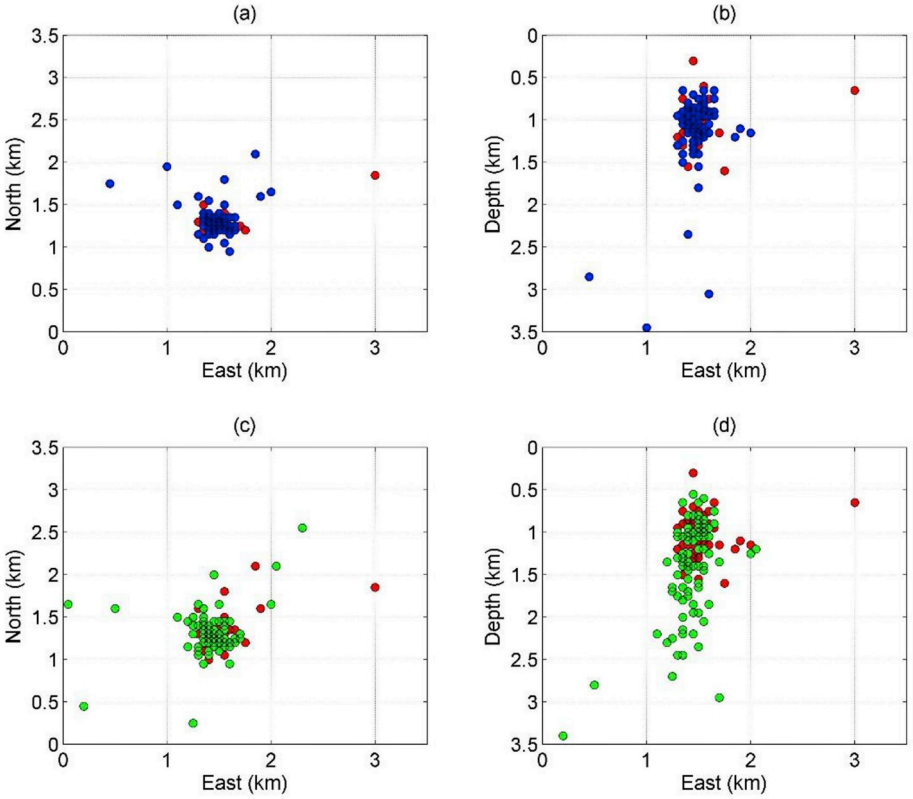

Fig. 9. Location results of DS with PSO (a)(b) and NA (c)(d). Red dots are results with FGS, blue and green dots are results of PSO and NA, respectively. (For interpretation of the references to color in this figure legend, the reader is referred to the Web version of this article.)

other issues, such as the SNR, the source-receiver geometry, the velocity model, also affect the location result. For field microseismic monitoring associated with hundreds or thousands of receivers in large surface arrays, we can even save thousands of seconds for locating a single event (Li et al., 2017). The studied stochastic algorithms, along with the proposed parameter tuning workflow, are also suitable for source mechanism inversion and joint microseismic inversion. For instance, Tan et al. (2018b) has successfully applied NA in source mechanism determination for induced seismicity. An advantage of NA is that it involves only two control parameters, which can be tuned more simply and easily. Based on our workflow, we believe NA and other optimization algorithms will perform better. However, optimized parameters from one problem or dataset are not recommended being directly applied to another one.

From an algorithmic point of view, the convergence performance is determined by the exploration-exploitation tradeoff. Increasing the number of candidates (*NP*) and generations (*NG*) can improve the convergence robustness by enhancing the exploration ability, while it decreases the computational efficiency by involving increased number of fitness function evaluations. This can be also regarded as robustness-efficiency tradeoff. Parameter tuning is supposed to control the exploration-exploitation tradeoff in an improved way, thus improve the overall performance of optimization algorithms. In this work, we take established stochastic optimization algorithms with limited ranges of control parameters. There are many modified versions of these algorithms available (e.g. Yang et al., 2007; Wathelet, 2008; Das and Suganthan, 2011). It is probably impossible to obtain a set of universal control parameters that work well in all cases. Following empirical procedure and the proposed parameter tuning workflow, stochastic optimization algorithms could be incorporated with microseismic location more efficiently.

Declarations of interest

None.

Authorship statement

L. Li contributed to method development and testing, and drafted the manuscript. J. Tan contributed to manuscript review and funding acquisition. Y. Xie and Y. Tan contributed to algorithm implementation of the study. J. Walda and Z. Zhao revised the manuscript carefully. D. Gajewski advised the study design and revised the manuscript.

Acknowledgements

We thank HMANET Project and Dirk Becker for providing the dataset. We are grateful to two anonymous reviewers and the editors for their constructive reviews and comments. The work is sponsored by Innovation-driven Project of Central South University (Grant No. 502501005), the National Natural Science Foundation of China (Grant No. 41872151) and the Open Research Fund Program of Key Laboratory of Metallogenic Prediction of Nonferrous Metals and Geological Environment Monitoring (Central South University), Ministry of Education (Grant No. 2018YSJS03). The reference source codes of microseismic location with stochastic algorithms are available in MATLAB on GitHub at https://github.com/leileely/microseismic_stochastic.

Appendix C. Supplementary data

Supplementary data to this article can be found online at https://doi.org/10.1016/j.cageo.2019.01.002.

Appendix A. Pseudo-codes of the three stochastic optimization algorithms for microseismic location

Algorithm 1: Particle Swarm Optimization (PSO) for microseismic location

1: Procedure PSO_ML (w, c_1, c_2, NP, NG)
2: Initialize velocities $\mathbf{v}_i$ and source parameters $\mathbf{x}_i$, where $i = 1,2, \cdots NP$
3: Initialize personal best parameter vector $\mathbf{P}_i$ and global best parameter vector $\mathbf{G}$
4: Calculate imaging function $S(\mathbf{x}_i)$
5: Find the best personal and global imaging value $S_{pbest}(\mathbf{x}_i)$, $S_{gbest}(\mathbf{x})$and the parameter vector $\mathbf{P}_i$, $\mathbf{G}$
6: For $k < NG$
7: $\mathbf{v}_i^k = w\mathbf{v}_i^{k-1} + c_1 r_1(\mathbf{P}_i^{k-1} - \mathbf{x}_i^{k-1}) + c_2 r_2(\mathbf{G}^{k-1} - \mathbf{x}_i^{k-1})$ ▷update velocities
8: $\mathbf{x}_i^k = \mathbf{x}_i^{k-1} + \mathbf{v}_i^k$ ▷update source parameters
9: If $S(\mathbf{x}_i) > S_{pbest}(\mathbf{x}_i)$
10: $S_{pbest}(\mathbf{x}_i) \leftarrow S(\mathbf{x}_i)$; $\mathbf{P}_i^k \leftarrow \mathbf{x}_i$ ▷update best personal imaging value and the parameter vector
11: End If
12: Update $S_{gbest}(\mathbf{x})$, $\mathbf{G}^k$
13: End For

Algorithm 2: Differential Evolution (DE) for microseismic location

1: Procedure DE_ML (F, CR, NP, NG)
2: Initialize source parameters $\mathbf{x}_i$, where $i = 1,2, \cdots NP$
3: Initialize personal best parameter vector $\mathbf{P}_i$ and global best parameter vector $\mathbf{G}$
4: Calculate imaging function $S(\mathbf{x}_i)$
5: Find the best personal and global imaging value $S_{pbest}(\mathbf{x}_i)$, $S_{gbest}(\mathbf{x})$and the parameter vector $\mathbf{P}_i$, $\mathbf{G}$
6: For $k < NG$
7: For $i < NP$
8: Pick three distinct numbers p_1, p_2 and p_3
9: Generate an integer L within $[1 \ \ P]$ ▷P is the number of source parameters
10: If $rand < CR$ or $j = L$ ▷$rand$ is a random number within $[0 \ 1]$, j is the source parameter index
11: $\mathbf{m}_i^k = \mathbf{x}_{p1}^k + F(\mathbf{x}_{p2}^k - \mathbf{x}_{p3}^k)$ ▷mutation and crossover, $\mathbf{m}$ is the competing population
12: else
13: $\mathbf{m}_i^k = \mathbf{x}_i^k$
14: End If
15: If $S(\mathbf{m}_i) > S(\mathbf{x}_i)$ ▷selection by one-to-one competing strategy
16: $S_{pbest}(\mathbf{x}_i) \leftarrow S(\mathbf{m}_i)$; $\mathbf{P}_i^k \leftarrow \mathbf{m}_i$
17: End if
18: End For
19: Update $S_{gbest}(\mathbf{x})$, $\mathbf{G}^k$
20: End For

Algorithm 3: Neighbourhood Algorithm (NA) for microseismic location

1: Procedure NA_ML (n_r, NP, NG)
2: Initialize source parameters $\mathbf{x}_i$, where $i = 1,2, \cdots NP$
3: Calculate imaging function $S(\mathbf{x}_i)$
4: Determine the n_r candidates with the maximum imaging value among all candidates generated so far
5: Generate NP new candidates by random walking in the n_rVoronoi cells (NP/n_rcandidates in each cell)
6: $\mathbf{x}_i \cong \min\{\mathbf{V}_{n_r}\} + rand \cdot (\max\{\mathbf{V}_{n_r}\} - \min\{\mathbf{V}_{n_r}\})$ ▷$rand$ is a random number within $[0 \ 1]$, $\mathbf{V}$ is the Voronoi cell space
7: Update the best global imaging value $S_{gbest}(\mathbf{x})$and the parameter vector $\mathbf{G}$
8: For $k < NG$
9: Repeat steps 3–7
10: End For

Appendix B. Complete results of SR and speedup in this work.

Table B.6
Results of SR (%) for CCS of a single field event.

NP	PSO						DE						NA			
	NG (w = 0.7)			NG (w = 1: (1-0.3)/NG:0.3)			NG (F = 0.5 CR = 0.5)			NG (F = 0.5 CR = 0.9)			NG (nr = 25)		NG (nr = 50)	
	30	50	100	30	50	100	30	50	100	30	50	100	30	50	30	50
30	76	100	100	99	100	100	66	100	100	91	100	100	\	\	\	\
50	98	100	100	100	100	100	79	100	100	99	100	100	99	100	93	100
100	100	100	100	100	100	100	92	100	100	100	100	100	100	100	100	100
250	100	100	100	100	100	100	100	100	100	100	100	100	100	100	100	100
550	100	100	100	100	100	100	100	100	100	100	100	100	100	100	100	100
1000	100	100	100	100	100	100	100	100	100	100	100	100	100	100	100	100

Table B.7
Results of SR (%) for CCS of 100 field events.

NP	PSO						DE						NA			
	NG (w = 0.7)			NG (w = 1: (1-0.3)/NG:0.3)			NG (F = 0.5 CR = 0.5)			NG (F = 0.5 CR = 0.9)			NG (nr = 25)		NG (nr = 50)	
	30	50	100	30	50	100	30	50	100	30	50	100	30	50	30	50
30	81	100	100	99	99	100	57	100	100	93	100	100	\	\	\	\
50	98	100	100	98	100	100	82	100	100	98	100	100	100	100	97	100
100	99	100	100	100	100	100	96	100	100	100	100	100	100	100	100	100
250	99	100	100	100	100	100	99	100	100	100	100	100	99	99	100	100
550	100	100	100	100	100	100	100	100	100	100	100	100	99	100	100	100
1000	100	100	100	100	100	100	100	100	100	100	100	100	100	100	100	100

Table B.8
Results of SR (%) for DS of a single field event.

NP	PSO						DE						NA			
	NG (w = 0.7)			NG (w = 1: (1-0.3)/NG:0.3)			NG (F = 0.5 CR = 0.5)			NG (F = 0.5 CR = 0.9)			NG (nr = 25)		NG (nr = 50)	
	30	50	100	30	50	100	30	50	100	30	50	30	50	30	50	
30	1	1	16	2	4	3	0	0	6	0	10	\	\	\	\	
50	0	7	15	1	12	8	0	0	4	0	8	3	13	1	9	
100	0	16	46	5	17	31	0	0	3	0	8	8	9	15	15	
250	12	43	59	25	48	57	0	0	4	1	10	9	14	21	16	
550	25	65	73	55	57	67	0	0	14	1	27	17	22	20	18	
1000	47	70	72	64	69	72	0	0	28	1	42	16	9	25	23	

Table B.9
Results of SR (%) for DS of 100 field events.

NP	PSO						DE						NA			
	NG (w = 0.7)			NG (w = 1: (1-0.3)/NG:0.3)			NG (F = 0.5 CR = 0.5)			NG (F = 0.5 CR = 0.9)			NG (nr = 25)		NG (nr = 50)	
	30	50	100	30	50	100	30	50	100	30	50	100	30	50	30	50
30	0	2	14	1	1	6	0	0	6	0	4	92	\	\	\	\
50	0	10	21	1	9	15	0	1	3	0	5	97	7	9	0	19
100	4	35	49	8	19	36	0	0	5	0	9	98	11	10	20	15
250	19	59	74	28	51	71	0	0	10	0	17	99	14	12	13	22
550	36	79	81	70	81	81	0	0	14	0	33	99	16	20	25	30
1000	65	83	91	71	84	87	0	0	23	0	35	100	26	14	29	21

Table B.10
Results of SR (%) for CCS of a single synthetic event using only S-waves.

NP	PSO						DE						NA			
	NG (w = 0.7)			NG (w = 1: (1-0.3)/NG:0.3)			NG (F = 0.5 CR = 0.5)			NG (F = 0.5 CR = 0.9)			NG (nr = 25)		NG (nr = 50)	
	30	50	100	30	50	100	30	50	100	30	50	100	30	50	30	50
30	96	100	100	69	97	97	6	93	100	61	100	100	\		\	\
50	98	100	100	81	99	99	5	99	100	77	100	100	100	100	100	100
100	100	100	100	98	100	100	14	100	100	90	100	100	100	100	100	100
250	100	100	100	100	100	100	16	100	100	100	100	100	100	100	100	100
550	100	100	100	100	100	100	25	100	100	100	100	100	100	100	100	100
1000	100	100	100	100	100	100	61	100	100	100	100	100	100	100	100	100

Table B.11
Results of SR (%) for DS of a single synthetic event using only S-waves.

NP	PSO						DE						NA			
	NG (w = 0.7)			NG (w = 1: (1-0.3)/NG:0.3)			NG (F = 0.5 CR = 0.5)			NG (F = 0.5 CR = 0.9)			NG (nr = 25)		NG (nr = 50)	
	30	50	100	30	50	100	30	50	100	30	50	100	30	50	30	50
30	2	15	20	1	3	27	0	0	0	0	0	68	\	\	\	\
50	3	19	32	0	10	25	0	0	0	0	0	78	4	12	1	11
100	13	35	34	0	29	37	0	0	0	0	0	76	9	11	17	33
250	50	45	63	9	44	35	0	0	0	0	0	84	21	20	31	32
550	54	67	71	34	56	54	0	0	0	0	0	86	16	24	34	42
1000	73	72	80	51	61	64	0	0	0	0	0	98	22	23	40	30

Table B.12
Speedup of three algorithms for CCS and DS.

NP	CCS (~2.6 s)								DS (~88.9 s)							
	PSO			DE			NA		PSO			DE			NA	
	30	50	100	30	50	100	30	50	30	50	100	30	50	100	30	50
30	260.00	130.00	52.00	260.00	130.00	65.00	\	\	21.17	13.07	6.68	2963.33	2222.50	1778.00	\	\
50	130.00	65.00	32.50	130.00	65.00	32.50	13.00	8.67	21.17	13.07	6.68	2222.50	1778.00	1270.00	20.67	12.70
100	65.00	37.14	20.00	52.00	32.50	15.29	6.50	2.89	21.17	13.07	6.68	1481.67	1111.25	683.85	18.91	10.98
250	28.89	17.33	8.67	16.25	9.63	4.81	1.44	0.58	21.17	13.07	6.68	683.85	423.33	222.25	13.07	6.35
550	13.68	8.39	4.19	4.91	2.92	1.46	0.35	0.14	21.17	13.07	6.68	197.56	120.14	76.64	5.63	2.48
1000	7.88	4.73	2.41	1.73	1.03	0.51	0.12	0.05	21.17	13.07	6.68	66.84	39.87	20.11	2.28	0.86

Table B.13
Location uncertainty of a sample field event with FGS and three optimization algorithms for CCS and DS.

NP	CCS (83.57 m)								DS (378.59 m)							
	PSO			DE			NA		PSO			DE			NA	
	30	50	100	30	50	100	30	50	30	50	100	30	50	100	30	50
30	89.70	79.09	76.00	96.09	84.18	82.14	\	\	1522.86	1650.22	1382.90	1480.13	835.44	326.14	\	\
50	81.37	78.31	85.67	84.06	82.14	84.51	79.76	89.55	1409.06	1296.82	1233.05	1412.18	885.58	242.69	1310.97	1119.94
100	81.84	84.51	80.29	84.71	80.58	80.52	79.50	82.20	1199.32	1298.45	1276.24	1363.00	834.21	249.57	1105.50	1093.89
250	87.51	83.31	83.33	86.13	84.56	81.60	76.55	81.08	963.13	987.37	1085.79	1304.54	796.03	276.22	897.61	923.56
550	83.57	80.46	81.70	84.48	81.76	90.12	91.58	80.20	771.91	725.13	781.34	1243.52	739.17	272.78	837.62	834.97
1000	80.65	82.79	82.36	82.43	91.61	83.70	82.72	84.26	721.26	587.58	652.19	1180.40	717.64	268.71	779.02	714.33

References

Allen, R.V., 1978. Automatic earthquake recognition and timing from single traces. Bull. Seismol. Soc. Am. 68 (5), 1521–1532.

Bischoff, S.T., Fischer, L., Wehling-Benatelli, S., Fritschen, R., Meier, T., Friederich, W., 2010. Spatio-temporal characteristics of mining induced seismicity in the eastern Ruhr-area. In: Proceedings of the Cahiers du Centre Europe en de Geodynamics et de Seismologie.

Brunini, G.I., Sabbione, J.I., Velis, D.R., 2017. Differential evolution for microseismic event location. In: Proceedings of the Information Processing and Control (RPIC), 2017 XVII Workshop on, pp. 1–6.

Das, S., Suganthan, P.N., 2011. Differential evolution: a survey of the state-of-the-art. IEEE Trans. Evol. Comput. 15 (1), 4–31.

Drew, J., White, R.S., Tilmann, F., Tarasewicz, J., 2013. Coalescence microseismic mapping. Geophys. J. Int. 195 (3), 1773–1785.

Duncan, P.M., Eisner, L., 2010. Reservoir characterization using surface microseismic monitoring. Geophysics 75 (5) 75A139-75A146.

Eiben, A.E., Hinterding, R., Michalewicz, Z., 1999. Parameter control in evolutionary algorithms. IEEE Trans. Evol. Comput. 3 (2), 124–141.

Eiben, A.E., Smit, S.K., 2011. Parameter tuning for configuring and analyzing evolutionary algorithms. Swarm Evol. Comput. 1 (1), 19–31.

Gajewski, D., Tessmer, E., 2005. Reverse modelling for seismic event characterization. Geophys. J. Int. 163 (1), 276–284.

Gajewski, D., Anikiev, D., Kashtan, B., Tessmer, E., 2007. Localization of seismic events by diffraction stacking. In: Proceedings of the 2007 SEG Annual Meeting, pp. 1287–1291.

Gharti, H.N., Oye, V., Roth, M., Kühn, D., 2010. Automated microearthquake location using envelope stacking and robust global optimization automated microearthquake location. Geophysics 75 (4), MA27–MA46.

Grechka, V., Heigel, W.M., 2017. Microseismic Monitoring. Society of Exploration Geophysicists, Tulsa, pp. 471pp.

Grigoli, F., Cesca, S., Amoroso, O., Emolo, A., Zollo, A., Dahm, T., 2014. Automated seismic event location by waveform coherence analysis. Geophys. J. Int. 196 (3), 1742–1753.

Grigoli, F., Cesca, S., Krieger, L., Kriegerowski, M., Gammaldi, S., Horalek, J., et al., 2016. Automated microseismic event location using Master-Event Waveform Stacking. Sci. Rep. 6.

Grigoli, F., Scarabello, L., Böse, M., Weber, B., Wiemer, S., Clinton, J.F., 2018. Pick-and waveform-based techniques for real-time detection of induced seismicity. Geophys. J. Int. 213 (2), 868–884.

Hassanil, H., Hloušek, F., Alexandrakis, C., Buske, S., 2018. Migration-based microseismic event location in the Schlema-Alberoda mining area. Int. J. Rock Mech. Min. Sci. 110, 161–167.

Kao, H., Shan, S.J., 2004. The source-scanning algorithm: mapping the distribution of seismic sources in time and space. Geophys. J. Int. 157 (2), 589–594.

Kennedy, R., Eberhart, R., 1995. Particle swarm optimization. In: Proceedings of the IEEE International Conference on Neural Networks.

Kennett, B.L.N., Marson-Pidgeon, K., Sambridge, M.S., 2000. Seismic Source characterization using a neighbourhood algorithm. Geophys. Res. Lett. 27 (20), 3401–3404.

Lagos, S.R., Sabbione, J.I., Velis, D.R., 2014. Very fast simulated annealing and particle swarm optimization for microseismic event location. In: Proceedings of the 2014 SEG Annual Meeting, pp. 2188–2192.

Lagos, S.R., Velis, D.R., 2018. Microseismic event location using global optimization

algorithms: an integrated and automated workflow. J. Appl. Geophys. 149, 18–24.
Li, L., Xie, Y.J., Chen, H., Wang, X.M., Gajewski, D., 2017. Improving the efficiency of microseismic imaging with particle swarm optimization. In: Proceedings of the 79th EAGE Conference and Exhibition 2017, We B4 11.
Li, L., Becker, D., Chen, H., Wang, X., Gajewski, D., 2018a. A systematic analysis of correlation-based seismic location methods. Geophys. J. Int. 212 (1), 659–678.
Li, L., Xie, Y., Gajewski, D., Tan, Y., Tan, J., 2018b. Parameter tuning of differential evolution algorithm for microseismic location. In: Proceedings of the 2018 SEG Annual Meeting, pp. 3047–3051.
Li, L., Tan, J., Wood, D.A., Zhao, Z., Becker, D., Lyu, Q., et al., 2019. A review of the current status of induced seismicity monitoring for hydraulic fracturing in unconventional tight oil and gas reservoirs. Fuel Accepted Manuscript. https://doi.org/10.1016/j.fuel.2019.01.026.
Luu, K., Noble, M., Gesret, A., Belayouni, N., Roux, P.-F., 2018. A parallel competitive Particle Swarm Optimization for non-linear first arrival traveltime tomography and uncertainty quantification. Comput. Geosci. 113, 81–93.
Lyu, Q., Long, X., Ranjith, P.G., Tan, J., Kang, Y., 2018a. Experimental investigation on the mechanical behaviours of a low-clay shale under water-based fluids. Eng. Geol. 233, 124–138.
Lyu, Q., Long, X., Ranjith, P.G., Tan, J., Kang, Y., Wang, Z., 2018b. Experimental investigation on the mechanical properties of a low-clay shale with different adsorption times in sub-/super-critical CO 2. Energy 147, 1288–1298.
Maity, D., Aminzadeh, F., Karrenbach, M., 2014. Novel hybrid artificial neural network based autopicking workflow for passive seismic data. Geophys. Prospect. 62 (4), 834–847.
Maity, D., Salehi, I., 2016. Neuro-evolutionary event detection technique for downhole microseismic surveys. Comput. Geosci. 86, 23–33.
Maxwell, S.C., 2014. Microseismic Imaging of Hydraulic Fracturing. Distinguished Instructor Series. Society of Exploration Geophysicists, Tulsa 214pp.
Oye, V., Roth, M., 2003. Automated seismic event location for hydrocarbon reservoirs. Comput. Geosci. 29 (7), 851–863.
Pei, D., Quirein, J.A., Cornish, B.E.Q., Quinn, D., Warpinski, N.R., 2009. Velocity calibration for microseismic monitoring: a very fast simulated annealing (VFSA) approach for joint-objective optimization. Geophysics 74 (6), WCB47–WCB55.
Pesicek, J.D., Child, D., Artman, B., Cieślik, K., 2014. Picking versus stacking in a modern microearthquake location: comparison of results from a surface passive seismic monitoring array in Oklahoma. Geophysics 79 (6), KS61–KS68.
Poiata, N., Satriano, C., Vilotte, J.-P., Bernard, P., Obara, K., 2016. Multiband array detection and location of seismic sources recorded by dense seismic networks. Geophys. J. Int. 205 (3), 1548–1573.
Ružek, B., Kvasnička, M., 2001. Differential evolution algorithm in the earthquake hypocenter location. Pure Appl. Geophys. 158 (4), 667–693.
Sambridge, M., 1999. Geophysical inversion with a neighbourhood algorithm—I. Searching a parameter space. Geophys. J. Int. 138 (2), 479–494.
Shapiro, S.A., 2015. Fluid-induced Seismicity. Cambridge University Press.
Shaw, R., Srivastava, S., 2007. Particle swarm optimization: a new tool to invert geophysical data. Geophysics 72 (2), F75–F83.
Sheng, G.Q., Li, Z.C., Wang, W.B., Wang, Z.Y., Zhu, H.W., Peng, G.M., 2014. A source location method for microseismic monitoring based on particle swarm optimization combined with differential evolution algorithm. Acta Pet. Sin. 35 (6), 1172–1181 [in Chinese].
Shi, Y., Eberhart, R., 1998. A modified particle swarm optimizer. In: Proceedings of the the 1998 IEEE International Conference on Evolutionary Computation, pp. 69–73.
Song, W.Q., Gao, Y.K., Zhu, H.W., 2013. The differential evolution inversion method based on Bayesian theory for micro-seismic data. Chin. J. Geophys. 56 (4), 1331–1339 [in Chinese].
Storn, R., Price, K., 1997. Differential evolution–a simple and efficient heuristic for global optimization over continuous spaces. J. Global Optim. 11 (4), 341–359.
Tan, Y., He, C., Mao, Z., 2018a. Microseismic velocity model inversion and source location: the use of neighborhood algorithm and master station method. Geophysics 83 (4), 1–15.
Tan, Y., Zhang, H., Li, J., Yin, C., Wu, F., 2018b. Focal mechanism determination for induced seismicity using the neighbourhood algorithm. Geophys. J. Int. 214 (3), 1715–1731.
Trelea, I.C., 2003. The particle swarm optimization algorithm: convergence analysis and parameter selection. Inf. Process. Lett. 85 (6), 317–325.
Verdon, J.P., Kendall, J., Hicks, S.P., Hill, P., 2017. Using beamforming to maximise the detection capability of small, sparse seismometer arrays deployed to monitor oil field activities. Geophys. Prospect (in press).
Walda, J., Gajewski, D., 2017. Determination of wavefront attributes by differential evolution in the presence of conflicting dips. Geophysics 82 (4), V229–V239.
Wathelet, M., 2008. An improved neighborhood algorithm: parameter conditions and dynamic scaling. Geophys. Res. Lett. 35 (9).
Wuestefeld, A., Näsholm, S., Greve, S., 2018. How the choice of location algorithm affect results: a synthetic comparison. In: Proceedings of the Seventh EAGE Workshop on Passive Seismic 2018.
Xie, Y., Gajewski, D., 2017. 5-D interpolation with wave-front attributes. Geophys. J. Int. 211 (2), 897–919.
Xue, Q., Wang, Y., Zhan, Y., Chang, X., 2015. An efficient GPU implementation for locating micro-seismic sources using 3D elastic wave time-reversal imaging. Comput. Geosci. 82, 89–97.
Yang, X.-S., 2010. Nature-inspired Metaheuristic Algorithms. Luniver press.
Yang, X., Yuan, J., Yuan, J., Mao, H., 2007. A modified particle swarm optimizer with dynamic adaptation. Appl. Math. Comput. 189 (2), 1205–1213.
Zeng, X., Zhang, H., Zhang, X., Wang, H., Zhang, Y., Liu, Q., 2014. Surface microseismic monitoring of hydraulic fracturing of a shale-gas reservoir using short-period and broadband seismic sensors. Seismol Res. Lett. 85 (3), 668–677.
Zhang, J., Zhang, H., Yu, J., Liu, Q., 2014. Fast one-dimensional velocity model determination using station-pair differential times based on the differential evolution method in microseismic monitoring. In: Proceedings of the 2014 SEG Annual Meeting, pp. 4832–4836.
Zimmer, U., Jin, J., 2011. Fast search algorithms for automatic localization of microseismic events. CSEG Recorder 36, 40–46.